



Sodankylä ionospheric tomography data set 2003–2014

Johannes Norberg^{1,2}, Lassi Roininen^{2,3}, Antti Kero², Tero Raita², Thomas Ulich², Markku Markkanen⁴,
Liisa Juusola¹, and Kirsti Kauristie¹

¹Finnish Meteorological Institute, Helsinki, Finland

²Sodankylä Geophysical Observatory, University of Oulu, Sodankylä, Finland

³Department of Mathematics, Tallinn University of Technology, Tallinn, Estonia

⁴Eigenor Corporation, Sodankylä, Finland

Correspondence to: Johannes Norberg (johannes.norberg@fmi.fi)

Received: 16 November 2015 – Published in Geosci. Instrum. Method. Data Syst. Discuss.: 4 December 2015

Revised: 15 April 2016 – Accepted: 2 May 2016 – Published: 1 July 2016

Abstract. Sodankylä Geophysical Observatory has been operating a receiver network for ionospheric tomography and collecting the produced data since 2003. The collected data set consists of phase difference curves measured from COSMOS navigation satellites from the Russian Parus network (Wood and Perry, 1980) and tomographic electron density reconstructions obtained from these measurements. In this study vertical total electron content (VTEC) values are integrated from the reconstructed electron densities to make a qualitative and quantitative analysis to validate the long-term performance of the tomographic system. During the observation period, 2003–2014, there were three to five operational stations at the Fennoscandia sector. Altogether the analysis consists of around 66 000 overflights, but to ensure the quality of the reconstructions, the examination is limited to cases with descending (north to south) overflights and maximum elevation over 60°. These constraints limit the number of overflights to around 10 000. Based on this data set, one solar cycle of ionospheric VTEC estimates is constructed. The measurements are compared against the International Reference Ionosphere (IRI)-2012 model, F10.7 solar flux index and sunspot number data. Qualitatively the tomographic VTEC estimate corresponds to reference data very well, but the IRI-2012 model results are on average 40 % higher than that of the tomographic results.

tomography with low-Earth-orbit (LEO) satellites, the objective is to reconstruct the ionospheric electron density in a two-, three- or four-dimensional domain from ground-based measurements of beacon satellite radio signals. The measured quantity is the phase shift of the transmitted radio signal. The phase shift is proportional to the integrated number density of free electrons along the signal path; hence, the measurements can be modelled as line integrals of ionospheric electron density. As the measurement geometry cannot provide horizontal ray directions, the information provided on vertical structures is poor. This results in a limited angle tomography inverse problem, which requires some regularisation scheme to stabilise the problem. The method operated by the Sodankylä Geophysical Observatory (SGO), is carried out within the framework of Bayesian statistical inverse problems. The current method is reported by Markkanen et al. (1995). Stabilisation of the inverse problem is given with first-order difference priors with a Chapman profile used in weighting the variances in the altitude. In a more recent analysis development, a similar framework has been used with Gaussian–Markov random field approximations for proper prior covariance structures (Norberg et al., 2015). Bust and Mitchell (2008) provide a good overview on other commonly used methods and on overall development of the topic.

SGO has been producing ionospheric tomography measurements operationally since 2003. For the observation period 2003–2014, the data set consists of around one solar cycle of measurements. SGO's measurements are based on Russian polar orbiting COSMOS satellites equipped with dual-frequency 150/400 MHz beacon transmitters. The ge-

1 Introduction

The use of tomographic methods for ionospheric research was first suggested by Austen et al. (1988). In ionospheric

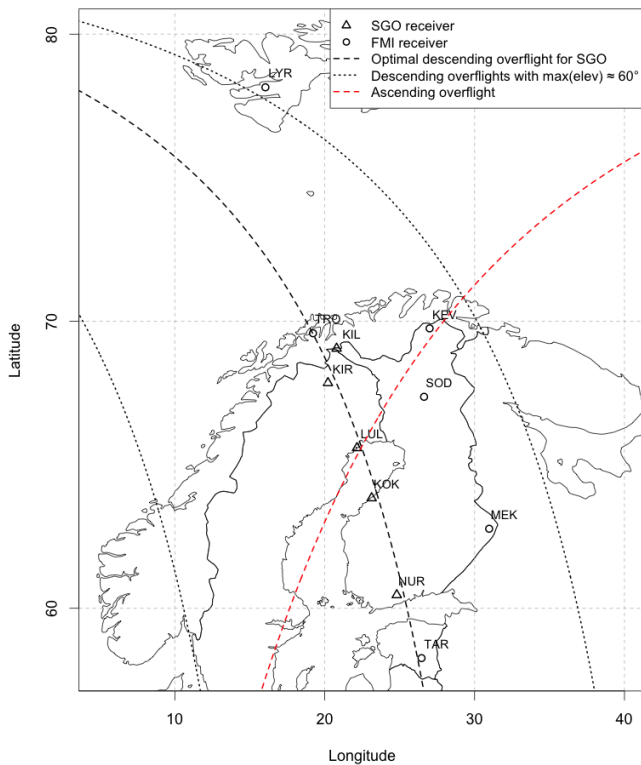


Figure 1. Current locations of SGO and FMI tomography chains.

ographical locations of the SGO chain are plotted in black triangles in Fig. 1. Recently, the Finnish Meteorological Institute (FMI), in collaboration with SGO, has installed six additional stations in the region allowing the observation area to expand from Tartu, Estonia to Longyearbyen, Svalbard, Norway, shown as black circles in Fig. 1. These TomoScand stations are able to receive signals from any beacon satellite transmitting at dual-frequency 150/400 MHz (Vierinen et al., 2014). For example the CASSIOPE/e-POP satellite mission has provided one new transmitter. A similar chain, operated by Polar Geophysical Institute, is on the Kolan peninsula and Karelia in north-west Russia (Kunitsyn and Tereshchenko, 2003). In this specific study, the SGO receiver chain and COSMOS satellites are considered.

The lack of horizontal measurements in ionospheric tomography causes well-known problems to reconstructions, especially when steep vertical gradients are involved. However, it was reported by Nygrén et al. (1996) that in the SGO algorithm, the local overestimations are usually compensated with local underestimations elsewhere, and vice versa; e.g. overestimation in layer thickness leads to reduced peak density. Hence, the solution for the absolute level, i.e. the total electron content (TEC) of relative electron density measurements is more stable than the actual profiles. To characterise the long-term trends in the ionosphere the TEC measurements are integrated vertically (vertical total electron content, VTEC) over each receiver station. Compressing the data

to an ionospheric VTEC value results in a more robust statistic and allows for more straightforward visualisation.

Typical choices for VTEC validation are GPS measurements. These methods are well-established, but due to the relatively low inclination of 55° , they do not measure directly the high-latitude ionosphere and provide information essentially southwards from the receiver sites. Therefore, when studying, e.g., travelling ionospheric disturbances at high latitudes, the wave structures can be distinguished in instantaneous snapshots but following their propagation is difficult (van de Kamp et al., 2014). Moreover, the GPS altitude is so high that the measurements include almost the entire plasmasphere. Especially at night-time, the plasmaspheric contribution to electron density can be significant. Jee et al. (2014) have performed similar studies for the last two solar minimum periods with TOPEX and JASON-1 satellites with orbital altitudes of 1337 km and inclination of 66.038° . From these satellites the VTEC can be solved as a by-product of altimetry estimation, but only over areas above the ocean.

The specific objective of this paper is to investigate the solar cycle variations in VTEC data obtained from the ionospheric tomography analysis. As reference material, the VTEC values derived from the IRI-2012 model (Bilitza et al. 2014), F10.7 solar flux index and sunspot number as extracted from NASA/GSFC's OMNI data set through OMNIWeb are used. By quantifying first the solar cycle variations in the data, the opportunities to use similar data also in studies on slower trends in high-latitude VTEC values can be considered. Based on model predictions, increased levels of carbon dioxide and methane are predicted to cool the thermosphere, and hence lower the so-called F2-peak layer; see e.g. Roble and Dickinson (1989). Indirect measurements of the height (hmF2) of the ionospheric F2 peak have been studied by a number of authors (see e.g. Bremer, 1992, 1998; Ulich and Turunen, 1997; Upadhyay and Mahajan, 1998; Cnossen and Franzke, 2014). The hmF2 values are derived empirically using routinely scaled ionograms. For detailed information on the hmF2 estimation in the Sodankylä Geophysical Observatory 1957–2014, see Roininen et al. (2015). In contrast to the hmF2 studies, the long-term TEC trends have not been widely studied. The first study was carried out by Lean et al. (2011), who considered GPS global and regional trends (1995–2010) with the main finding of slow increasing trends (0.6 ± 0.3 total electron content unit (TECU) decade⁻¹, TECU = 10^{16} Ne m⁻²) in the daily averaged global TEC values. One explanation for this trend could be a reduction in the upper atmospheric recombination rates due to cooling in the thermosphere. In the future, LEO tomography measurement could contribute to refining the result of Lean et al. (2011) at high latitudes where GPS measurements have accuracy problems due to oblique signal paths.

This paper is organised as follows: in Sect. 2 the SGO ionospheric tomographic data and the ionospheric VTEC estimation are overviewed. Section 3 includes a discussion of

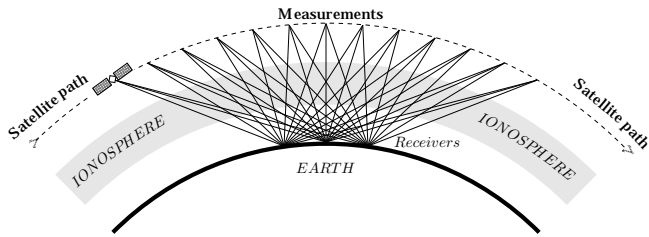


Figure 2. Schematic plot of ionospheric tomography with LEO beacon satellites.

the estimated VTEC and IRI-2012 model results. Section 4 concludes the study and provides some notes for future research.

2 Data and methodology

The ionospheric tomography reconstructions provided by SGO are solved in two-dimensional latitude–altitude domain. The orbital altitude of COSMOS satellites is approximately 1000 km and one such overflight takes approximately 10 min. The measurement geometry then resembles the schematic plot in Fig. 2. During the years 2003–2014, the number of operational satellites varied between three and seven. Most of the time four satellites have been providing transmissions. Figure 3 shows an example result sheet for one overflight from the SGO’s tomography web archive (<http://www.sgo.fi/Data/Tomography/tomoArchive.php>).

The inclination of COSMOS satellites is $\sim 83^\circ$, i.e. compared to a strictly polar orbit, the direction of the satellites is tilted slightly eastwards. The geographical locations of the receiver stations are Nurmijärvi (60.51° N , 24.65° E), Kokkola (63.83° N , 23.16° E), Luleå (65.62° N , 22.14° E), Kiruna (67.85° N , 20.41° E) and Kilpisjärvi (69.02° N , 20.86° E). At the beginning of the observation period, a station in the European Incoherent Scatter Scientific Association (EISCAT) site in Tromsø, Norway, was used, but this station was soon moved to Kilpisjärvi. The Nurmijärvi measurements started in June 2004. The SGO receivers are installed along the inclination angle so that the descending, i.e. southward, overflights are somewhat parallel to the chain. Figure 1 illustrates how in an optimal case the descending satellite trajectory is aligned with the chain, but also how the ascending, i.e. northward, overflights are almost perpendicular to the chain. In Fig. 4 the number of satellite overflights are plotted against satellite elevation.

Since in two-dimensional ionospheric tomography the longitudinal gradients cannot be taken into account, the set of reconstructions is limited to descending overflights with maximum elevation angles over 60° , when observed from the Kokkola station. To get an idea of the trajectories included in analysis, two extremes of descending overflights with maximum elevation angles close to 60° are shown in Fig. 1. Lim-

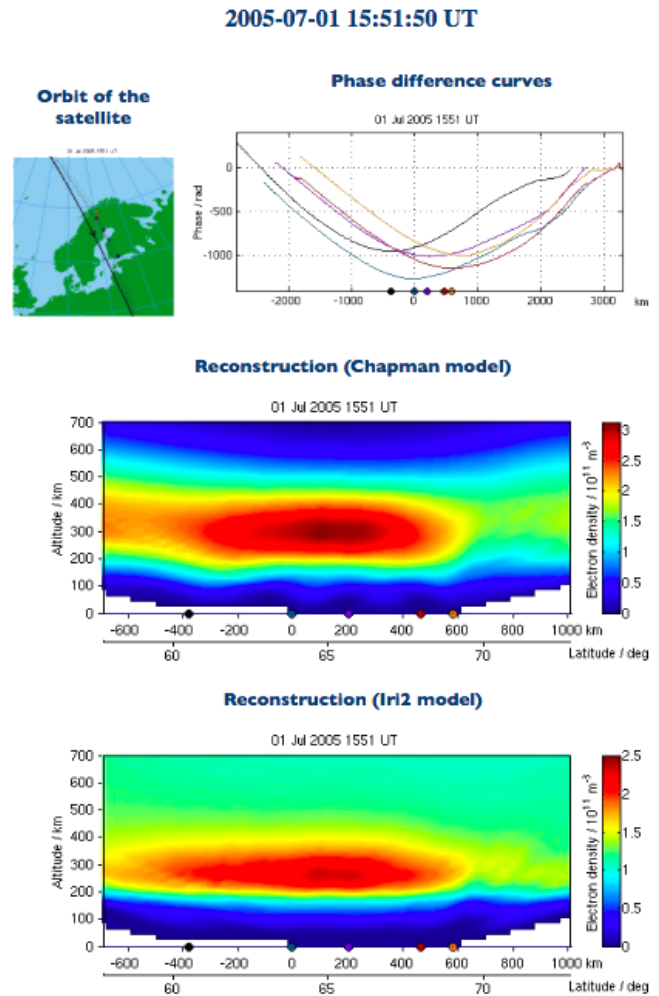


Figure 3. Tomographic reconstruction result from Sodankylä Geophysical Observatory. The satellite trajectory, observed phase difference curves and tomographic results with two different prior models. The receiver stations are shown as coloured points. The origin of the kilometre axis is placed on Kokkola station.

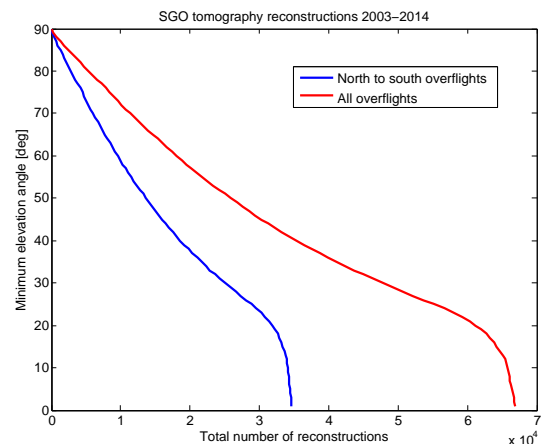


Figure 4. The number of satellite overflights over the whole observation period with respect to minimum threshold elevation.

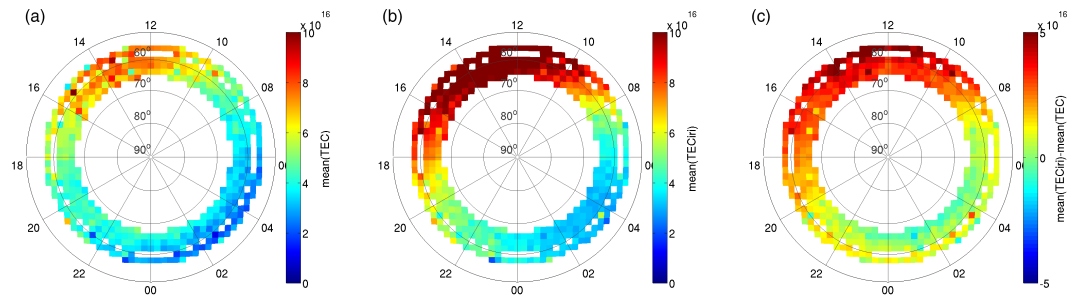


Figure 5. Magnetic local time mean values for tomographic VTEC, corresponding IRI-2012 values and the difference between the two.

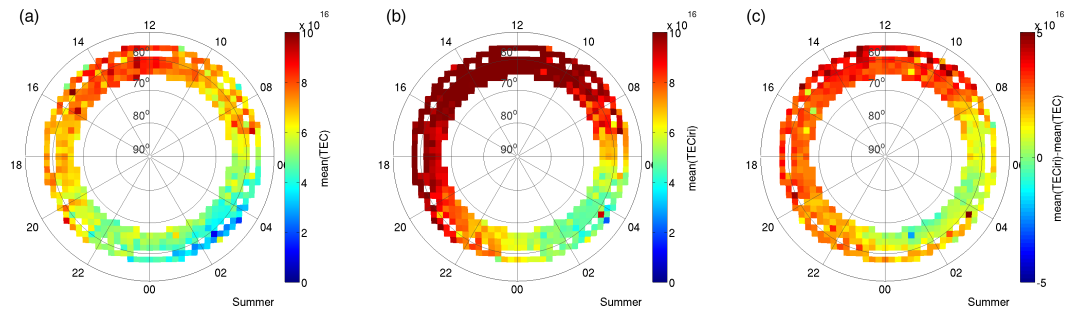


Figure 6. Magnetic local time mean values for summer time tomographic VTEC, corresponding IRI-2012 values and the difference between the two.

iting the original data of 66 000 overflights with these criteria results with a data set of around 10 000 tomographic reconstructions, on average a little more than two overflights per day. Instead of analysing complete two-dimensional reconstructions the data are simplified to ionospheric VTEC measurements. The VTEC is obtained by integrating the reconstructed electron densities above each SGO receiver from ground level to satellite altitude.

The reference data sets of IRI-2012 (http://omniweb.gsfc.nasa.gov/vitmo/iri2012_vitmo.html), F10.7 and sunspot (<http://omniweb.gsfc.nasa.gov/form/dx1.html>) number values are all collected with the same time axis as the tomographic VTEC data. The IRI-2012 VTEC values are integrated from the model results vertically between the altitudes 0–1000 km at the receiver locations, similarly to the tomographic VTEC.

3 Results and discussion

To characterise the data, they are first presented in Figs. 5–8 as averaged VTEC values in magnetic latitude and a magnetic local time (MLT) coordinate system. This is done separately for the complete and seasonal data sets from summer, equinox and winter. Winter is defined as one-third of a year centred around the winter solstice. Summer starts one-third of a year after winter solstice and lasts for one-third of a year. Everything else is defined as equinox. In Figs. 5–8 first the data for tomographic then for IRI-2012 VTEC values are

shown. The third image illustrates the differences between these two. In all Figs. 5–8 the relative diurnal behaviour in VTEC values within different seasons are relatively comparable between tomographic and IRI-2012 data. Both approaches show in dayside VTEC values a dawn–dusk asymmetry with higher values on the dusk side. This asymmetry is pronounced particularly during summer time in Fig. 6, where according to IRI-2012 enhanced VTEC values extend to pre-midnight hours. In the tomography results a similar trend is visible but the extension of high VTEC to night-time hours beyond 18:00 MLT is missing. In all seasons the electron densities are systematically higher in the IRI-2012 data, with the maximum difference close to 5 TECU. The difference plots show that the differences in summer, in Fig. 6, are slightly smaller than in equinox and winter seasons, in Figs. 7 and 8. In all Figs. 5–8, at the magnetic local night-time, the differences are in general somewhat smaller and both positive and negative. Figures 7 and 8 indicate that in equinox and winter at magnetic local night-time, the tomographic VTEC values at higher latitudes are larger than the corresponding values from the IRI-2012 model.

In order to deduce whether the solar cycle can be observed from the data, in Figs. 9 and 10 the data sets for the location of Kokkola station are presented as time series for the complete period of 2003–2014. Kokkola is chosen as the representative case as it is located close to the centre of the tomographic domain and also provides good operational coverage

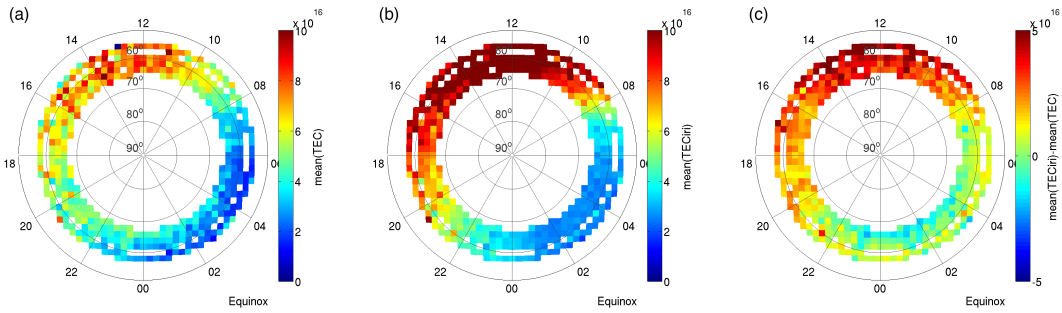


Figure 7. Magnetic local time mean values for equinox time tomographic VTEC, corresponding IRI-2012 values and the difference between the two.

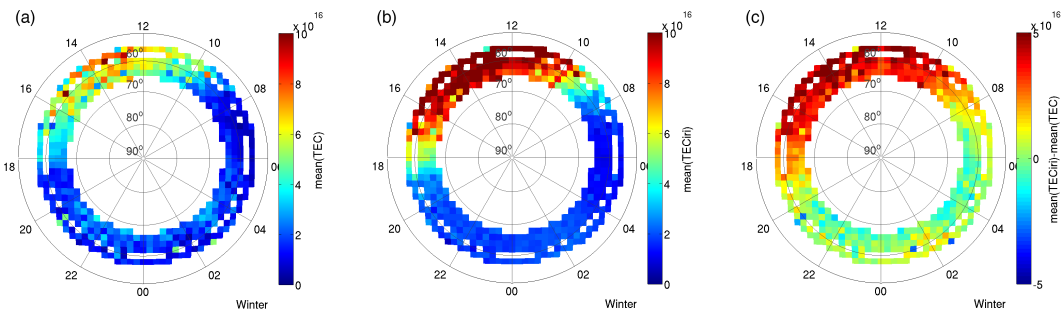


Figure 8. Magnetic local time mean values for winter time tomographic VTEC, corresponding IRI-2012 values and the difference between the two.

in the observation period. Furthermore, in illustrations of this kind, the large-scale features are the same for all stations.

In Fig. 9 the VTEC over Kokkola station is presented as monthly means for each MLT hour. This is done for the whole observation period. In the same figure the corresponding VTEC values from the IRI-2012 model and the differences between them are presented again. First, Fig. 9 shows the nature of satellite availability. The period of COSMOS satellites is 105 min, which produces a drift in daily times of overflights. The images also show a maxima of VTEC in 2003 and in 2014. Similarly to Figs. 5–8 the systematic differences between tomographic and IRI-2012 VTEC values are visible. IRI-2012 VTEC values are on average approximately 40 % higher than average tomographic VTEC.

The overestimation of high latitude Ne has been widely reported for different versions of IRI model. (Zhang et al., 2007) reported that IRI-2001 overestimates Ne at the peak altitude and above, especially in winter time compared to incoherent scatter radar (ISR) measurements. One of the main improvements for IRI-2007 was the topside Ne modelling (Bilitza and Reinisch, 2008). Lühr and Xiong (2010) compared the IRI-2007 model results to orbital averages of CHAMP and GRACE satellite measurements from 2000 to 2009, with the satellite height range from 300 to 500 km. Especially during the solar minimum period the overestimation was up to 60 %. The overestimation was concentrated on the lower latitudes, but in (Xiong et al., 2011) a 20 % overestimation also

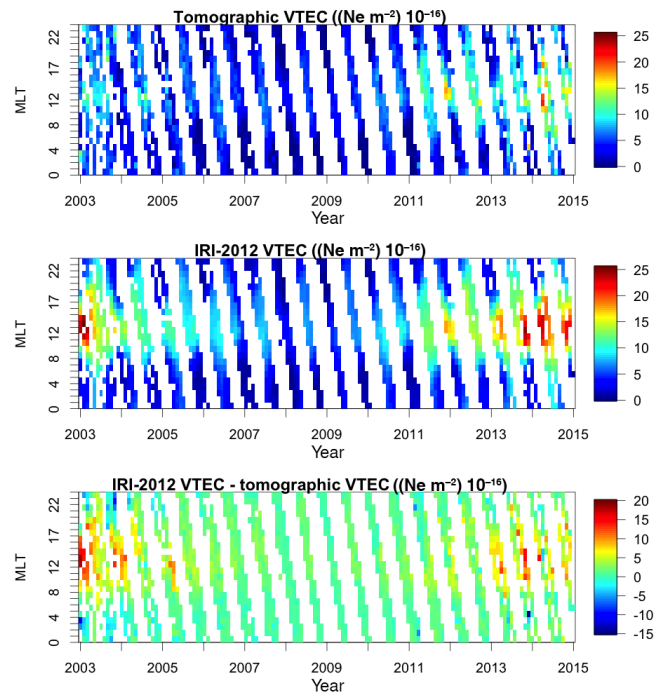


Figure 9. Monthly VTEC averages for each MLT hour over the Kokkola station.

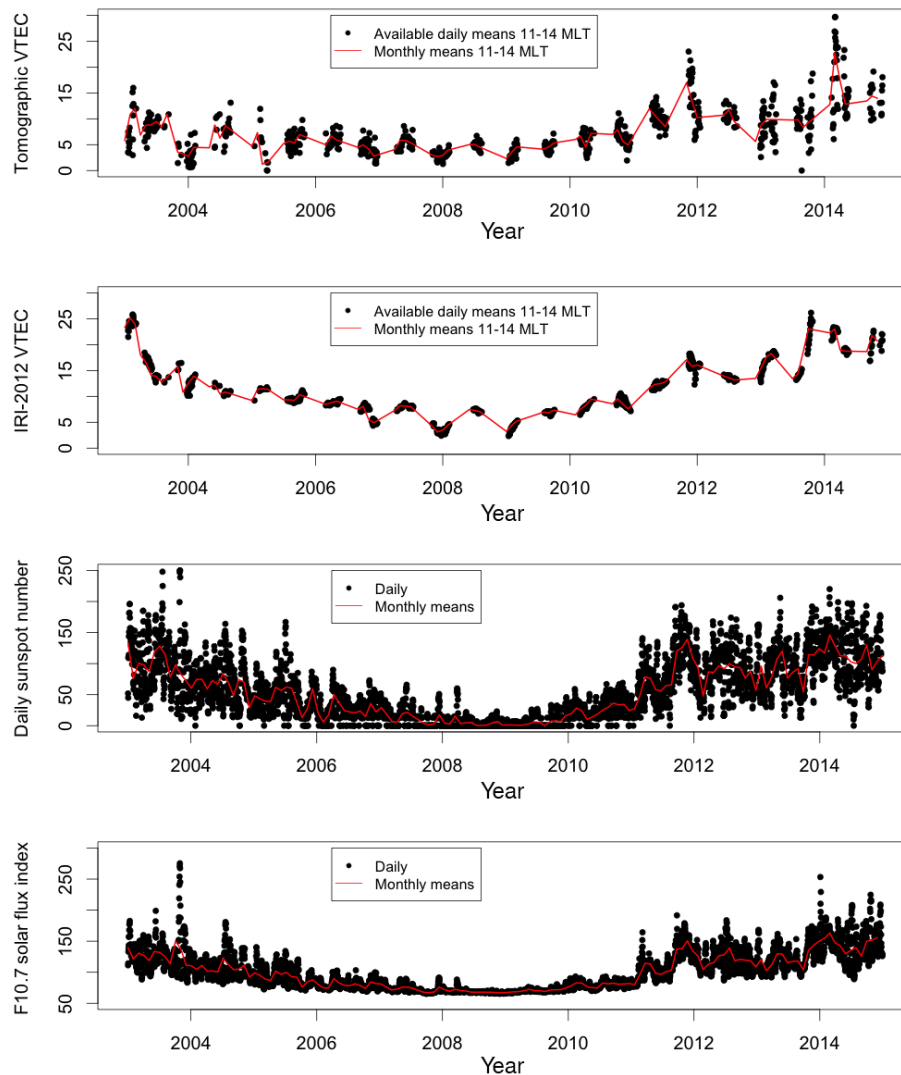


Figure 10. VTEC values over Kokkola averaged from 11:00 to 13:00 MLT vs. corresponding IRI-2012 model values, sunspot number and solar flux index F10.7.

for a trough area was reported. (Xiong et al., 2011) utilised CHAMP and GRACE satellite-based Ne measurements from 2005 to 2010.

These studies then suggested that despite the development, the modelling of F peak and topside Ne still contains some problems. The improvements for IRI-2012 were made for the thickness and the shape of the bottom-side F2 layer, as well as for the description of storm effects in the auroral E region (Bilitza et al., 2014).

We have found it difficult to find a comprehensive account of the different measurements used in the IRI model. In (Altadill et al., 2008) a network of 27 ionosondes were used for the enhanced bottom-side modelling of Ne. The closest ionosonde measurements to Fennoscandia in the network were from Chilton, UK. In all, the network comprises two high latitude ionosondes, both located in Greenland.

The Sodankylä tomographic set-up employs numerous measurements from the high-latitude area. However, ionospheric tomographic inversion is well-known to be an unstable inverse problem, and its performance, especially in small-scale details in vertical structures, can be argued. The Bayesian approach (Markkanen et al., 1995) utilised here assumes zero electron density a priori, and variations from zero background are then controlled with a Chapman profile shaped standard deviation. The approach is hence more likely to underestimate than overestimate the electron densities. Hence, if the system has a bias, it would be most likely towards zero.

A discernible exception for the systematic difference between IRI-2012 and tomographic VTEC is in the MLT hours around midnight of the year 2003 (blue pixels in the lowest panel of Fig. 9). It is known to be a year of particularly

strong space weather activity (see e.g. Juusola et al., 2015). Geomagnetic activity is strong particularly during 2–3 years after the solar maxima (Nevanlinna and Pulkkinen, 1998). Both 2003 and 2014 are such years. Geomagnetic activity is caused by processes in the night-side magnetosphere, which also generate enhanced electron and proton precipitation into the ionosphere. The impact of this precipitation is mostly visible in the E-layer densities. Our results suggest that IRI-2012, as a statistical model, cannot describe these special situations accurately, while the tomography inversion manages at least partly to catch the altitude integrated impact from this precipitation.

In Fig. 10, in addition to IRI-2012, the tomographic data are compared to the daily sunspot number and F10.7 solar flux index. Here only the midday (11–13:00 MLT) VTEC from Kokkola station and corresponding values from the IRI-2012 model were selected for the analysis. Due to a low number of satellites, the measurement times are not uniformly represented; i.e. some time slots are over-presented in the data. However, even despite non-uniformity of the data, the solar cycle dependence is clear. The pattern of tomographic VTEC corresponds essentially to reference data.

4 Conclusions

In this paper, the SGO's LEO-satellite ionospheric tomography data set from the period of 2003–2014 is presented. This data set covers approximately one solar cycle. The primary aim of this paper is to see the solar cycle effect in the data. For this purpose, the estimated VTEC values were used, which clearly exhibit similar solar cycle-dependent features than in sunspot number and solar flux index F10.7 data.

The tomographic VTEC values also have a relative agreement with the corresponding VTEC values obtained from the IRI-2012 model, but there is a systematic difference between the two. The values based on the IRI-2012 model are on average 40 % higher than those of the tomographic results. As an exception for the systematic difference, the results suggest that the tomographic results capture geomagnetic night-time activity in increased VTEC values.

Further studies are needed to resolve the reason for the significant discrepancy between the tomographic and IRI-2012 VTEC values. However, as mentioned in the Introduction, improved inversion methods for ionospheric tomography are under development. The upgrading work includes better methods to estimate the quality of inversion results. Therefore, we believe that beacon-based tomography could be used more intensively in future research, perhaps even in IRI validation and upgrading.

We suggest that the VTEC values from beacon-based tomographic inversion can constitute a viable tool for studying long-term trends in the atmosphere. The standard long-term trend is usually studied via the F2-layer peak. But as this is a point value, the overall VTEC can import some extra in-

formation to the analysis. However, as the data considered here consist of only one solar cycle, it is practically impossible to say anything about the long-term trends merely on the basis of the measured VTEC values. Hence, at least one extra cycle for a proper long-term VTEC trend analysis is required, as well as further studies to resolve the reason for the discrepancy with tomographic and IRI-based VTEC values.

Data availability

The IRI-2012 electron density profiles are available from IRI-2012 (http://omniweb.gsfc.nasa.gov/vitmo/iri2012_vitmo.html). The F10.7 solar flux and sunspot number data are available from OMNI 2 (<http://omniweb.gsfc.nasa.gov/form/dx1.html>). Ionospheric tomography measurements and analysed data products used in this paper are available upon request from the Sodankylä Geophysical Observatory. The quick-look plots are available online (<http://www.sgo.fi/Data/Tomography/tomoArchive.php>).

Acknowledgements. This work has been funded by European Regional Development Fund (Regional Council of Lapland, decision number A70179), Academy of Finland (decision number 287679) and European Research Council (ERC advanced grant 267700 – Inverse problems).

Edited by: N. Partamies

References

- Altadill, D., Torta, J. M., and Blanch, E.: Proposal of new models of the bottom-side B_0 and B_1 parameters for IRI, *Adv. Space Res.*, 43, 1825–1834, doi:10.1016/j.asr.2008.08.014, 2008.
- Austen, J. R., Franke, S. J., and Liu, C. H.: Ionospheric imaging using computerized tomography, *Radio Sci.*, 3, 299–307, 1988.
- Bilitza, D. and Reinisch, B.: The international reference ionosphere 2007: Improvements and new parameters, *Adv. Space Res.*, 42, 4, 599–609, doi:10.1016/j.asr.2007.07.048, 2008.
- Bilitza, D., Altadill, D., Zhang, Y., Mertens, C., Truhlik, V., Richards, P., McKinnell, L.-A., and Reinisch, B.: The international reference ionosphere 2012 – model of international collaboration, *Journal of Space Weather and Space Climate*, 4, A07, doi:10.1051/swsc/2014004, 2014.
- Bremer, J.: Ionospheric trends in mid-latitudes as a possible indicator of the atmospheric greenhouse effect, *J. Atmos. Terr. Phys.*, 54, 1505–1511, 1992.
- Bremer, J.: Trends in the ionospheric E and F regions over Europe, *Ann. Geophys.*, 16, 986–996, doi:10.1007/s00585-998-0986-9, 1998.
- Bust, G. S. and Mitchell, C. N.: History, current state, and future directions of ionospheric imaging, *Rev. Geophys.*, 46, RG1003, doi:10.1029/2006RG000212, 2008.
- Cnossen, I. and Franzke, C.: The role of the Sun in long-term change in the F2 peak ionosphere: new insights from EEMD and

- numerical modeling, *J. Geophys. Res.-Space*, 119, 8610–8623, 2014.
- F10.7 and solar flux data: NASA/GSFC's Space Physics Data Facility's OMNIWeb service, and OMNI data, Goddard Space Flight Center, NASA, available at: <http://omniweb.gsfc.nasa.gov/form/dx1.html>, last access: 20 May 2016.
- Ionospheric tomographic Quicklook: Ionospheric tomography measurements and analysed data products, Sodankylä Geophysical Observatory, Finland, available at: <http://www.sgo.fi/Data/Tomography/tomoArchive.php>, last access: 20 May 2016.
- IRI-2012: International Reference Ionosphere – IRI-2012 data, NASA, available at: http://omniweb.gsfc.nasa.gov/vitmo/iri2012_vitmo.html, last access: 20 May 2016.
- Jee, G., Lee, H.-B., Solomon, S. C., Cnossen, I., and Franzke, C.: Global ionospheric total electron contents (TECs) during the last two solar minimum periods, *J. Geophys. Res.-Space*, 119, 2090–2100, doi:10.1002/2013JA019407, 2014.
- Juusola, L., Viljanen, A., Van De Kamp, M., Tanskanen, E. I., Vanhamäki, H., Partamies, N., and Kauristie, K.: High-latitude ionospheric equivalent currents during strong space storms: regional perspective, *Space Weather*, 13, 49–60, doi:10.1002/2014SW001139, 2015.
- Kunitsyn, V. E. and Tereshchenko, E. D.: *Ionospheric Tomography*, Springer-Verlag, Berlin, Germany, 2003.
- Lean, J. L., Emmert, J. T., Picone, J. M., and Meier, R. R.: Global and regional trends in ionospheric total electron content, *J. Geophys. Res.*, 116, A00H04, doi:10.1029/2010JA016378, 2011.
- Lühr, H. and Xiong, C.: IRI-2007 model overestimates electron density during the 23/24 solar minimum, *Geophys. Res. Lett.*, 37, L23101, doi:10.1029/2010GL045430, 2010.
- Markkanen, M., Lehtinen, M., Nygrén, T., Pirttilä, J., Helenius, P., Vilenius, E., Tereshchenko, E. D., and Khudukon, B. Z.: Bayesian approach to satellite radiotomography with applications in the Scandinavian sector, *Ann. Geophys.*, 13, 1277–1287, 1995.
- Nevanlinna, H. and Pulkkinen, T. I.: Solar cycle correlations of substorm and auroral frequency, *Geophys. Res. Lett.*, 25, 3087–3090, 1998.
- Norberg, J., Roininen, L., Vierinen, J., Amm, O., McKay-Bukowski, D., and Lehtinen, M.: Ionospheric tomography in Bayesian framework with Gaussian Markov random field priors, *Radio Sci.*, 50, 138–152, doi:10.1002/2014RS005434, 2015.
- Nygrén, T., Markkanen, M., Lehtinen, M., Tereshchenko, E. D., Khudukon, B. Z., Evstafiev, O. V., and Pollari, P.: Comparison of F-region electron density observations by satellite radio tomography and incoherent scatter methods, *Ann. Geophys.*, 14, 1422–1428, doi:10.1007/s00585-996-1422-7, 1996.
- Roble, R. G. and Dickinson, R. E.: How will changes in carbon dioxide and methane modify the mean structure of the mesosphere and thermosphere, *Geophys. Res. Lett.*, 16, 1441–1444, doi:10.1029/GL016i012p01441, 1989.
- Roininen, L., Laine, M., and Ulich, T.: Time-varying ionosonde trend: Case study of Sodankylä $h_m F_2$ data 1957–2014, *J. Geophys. Res. Space*, 120, 6851–6859, doi:10.1002/2015JA021176, 2015.
- Ulich, T. and Turunen, E.: Evidence for long-term cooling of the upper atmosphere in ionosonde data, *Geophys. Res. Lett.*, 24, 1103–1106, 1997.
- Upadhyay, H. O. and Mahajan, K. K.: Atmospheric greenhouse effect and ionospheric trends, *Geophys. Res. Lett.*, 25, 3375–3378, 1998.
- van de Kamp, M., Pokhotelov, D., and Kauristie, K.: TID characterised using joint effort of incoherent scatter radar and GPS, *Ann. Geophys.*, 32, 1511–1532, doi:10.5194/angeo-32-1511-2014, 2014.
- Vierinen, J., Norberg, J., Lehtinen, M. S., Amm, O., Roininen, L., Väänänen, A., Erickson, P. J., and McKay-Bukowski, D.: Beacon satellite receiver for ionospheric tomography, *Radio Sci.*, 49, 1141–1152, doi:10.1002/2014RS005431, 2014.
- Wood, C. D. and Perry, G. E.: The Russian Satellite Navigation System, *Philos. T. Roy. Soc. A*, 294, 307–315, doi:10.1098/rsta.1980.0037, 1980.
- Xiong, C., Lüher, C., and Ma, S. Y.: The subauroral electron density trough: Comparison between satellite observations and IRI-2007 model estimates, *Adv. Space Res.*, 51, 536–544, doi:10.1016/j.asr.2011.09.021, 2011.
- Zhang, S.-R., Holt, J. M., Bilitza, D. K., van Eyken, T., McCready, M., Amory-Mazaudier, C., Shoichiro, F., and Sulzer, M.: Multiple-site comparisons between models of incoherent scatter radar and IRI, *Adv. Space Res.*, 39, 910–917, doi:10.1016/j.asr.2006.05.027, 2007.